


## Experimental Characterization of Photoemission from Plasmonic Nanogroove Arrays

Christopher M. Pierce<sup>1,2,\*</sup>, Daniel B. Durham,<sup>3</sup> Fabrizio Riminucci,<sup>1</sup> Scott Dhuey,<sup>1</sup> Ivan Bazarov,<sup>2</sup> Jared Maxson,<sup>2</sup> Andrew M. Minor,<sup>3</sup> and Daniele Filippetto<sup>1,†</sup>

<sup>1</sup>*Lawrence Berkeley National Laboratory (LBNL), 1 Cyclotron Road, Berkeley, California 94720, USA*

<sup>2</sup>*Cornell Laboratory for Accelerator-Based Sciences and Education (CLASSE), Cornell University, 161 Synchrotron Drive, Ithaca, New York 14853-8001, USA*

<sup>3</sup>*Department of Materials Science and Engineering, University of California, Berkeley, and National Center for Electron Microscopy, Molecular Foundry, Lawrence Berkeley National Laboratory, Berkeley, California 94720 USA*

 (Received 10 October 2022; revised 12 December 2022; accepted 15 February 2023; published 10 March 2023)

Metal photocathodes are an important source of high-brightness electron beams, ubiquitous in the operation of both large-scale accelerators and table-top microscopes. When the surface of a metal is nanoengineered with patterns on the order of the optical wavelength, it can lead to the excitation and confinement of surface-plasmon-polariton waves that drive nonlinear photoemission. In this work, we aim to evaluate gold plasmonic nanogrooves as a concept for producing bright electron beams for accelerators via nonlinear photoemission. We do this by first comparing their optical properties to numerical calculations from first principles to confirm our ability to fabricate these nanoscale structures. Their nonlinear photoemission yield is found by measuring emitted photocurrent as the intensity of their driving laser is varied. Finally, the mean transverse energy of this electron source is found using the solenoid-scan technique. Our data demonstrate the ability of these cathodes to provide a tenfold enhancement in the efficiency of photoemission over flat metals driven with a linear process. We find that these cathodes are robust and capable of reaching sustained average currents over 100 nA at optical intensities larger than  $2 \text{ GW cm}^{-2}$  with no degradation of performance. The emittance of the generated beam is found to be highly asymmetric, a fact we can explain with calculations involving the also asymmetric roughness of the patterned surface. These results demonstrate the use of nanoengineered surfaces as enhanced photocathodes, providing a robust air-stable source of high-average-current electron beams hopefully with great potential for industrial and scientific applications.

DOI: [10.1103/PhysRevApplied.19.034034](https://doi.org/10.1103/PhysRevApplied.19.034034)

### I. INTRODUCTION

High-brightness electron sources for ultrafast applications require prompt emission of high-charge electron beams and direct injection into areas of extreme electromagnetic field amplitudes. Photoemission from metal surfaces has been the primary means of electron bunch generation, used by the large majority of user facilities around the world [1–3], owing to their fast response time and robustness. Despite their broad use, metal cathodes have a few major disadvantages. First, the typical quantum efficiency for a metal exhibits values in the  $10^{-5}$  region which, for high-charge pulse extraction, requires laser-pulse intensities close to the damage threshold of the material. With time and continuous operation, this has been shown to lead to partial ablation, increased surface

roughness, and reduced brightness [4]. High intensities may also cause multiphoton absorption and photoemission, leading to the generation of unwanted halos, and an overall increase of beam thermal emittance [5]. Furthermore, a typical metal work function requires UV photons for linear photoemission. The two-stage UV conversion from the initial infrared laser pulses has a substantial impact on the size and complexity of the photocathode laser system. It may also impact the quality of the final pulse, resulting in substantial loss of energy, degradation of the transverse pulse shape, and limited control over the longitudinal profile. Altogether, the low quantum efficiency and the high work function effectively limit the maximum average current that can be extracted by metal cathodes and, therefore, the range of applications of the relevant instrumentation.

High-quantum-efficiency semiconductor films provide a possible path toward higher-performance photocathodes. Depending on the choice of the material, the quantum

\*[cmp285@cornell.edu](mailto:cmp285@cornell.edu)

†[dfilippetto@lbl.gov](mailto:dfilippetto@lbl.gov)

efficiency can be orders of magnitude larger for a work function in the visible or infrared region [6]. Unfortunately, such cathodes are chemically reactive and the vacuum levels found in high-field photoinjectors often greatly complicate their use as high-brightness electron sources. Further, dark current may become an issue in those same systems for materials with an extremely low work function.

Nonlinear photoemission may offer another potential solution to avoid nonlinear wavelength conversion. Depending on the material and laser parameters, it becomes more efficient to extract electrons from the cathode directly via multiphoton photoemission using infrared light, rather than perform wavelength conversion to the UV [7]. However, as is the case for linear photoemission, the small nonlinear yield of most flat metallic surfaces demands laser-fluence values close to the damage threshold of the material (typically on the order of 0.1 to 1 J cm<sup>-2</sup> [8]).

One path forward in improving the nonlinear yield of metals is by fabricating plasmonic structures by surface nanopatterning. Nanoscale grooves formed on a gold photocathode have been shown to increase its nonlinear yield at 800 nm by up to 6 orders of magnitude [9]. A similar concept using a grid of nanoscale holes has shown a dramatic increase in the nonlinear yield of gold and copper photocathodes [10,11]. On the other hand, many questions remain open before such cathodes can be effectively considered as a reliable source for ultrafast application. Can we produce nanoengineered cathodes with repeatable properties? How does the mean transverse energy of the extracted beam depend on the nanostructures? Can such structures provide stable high average currents for extended periods with no degradation?

In this work, we provide a detailed characterization of nanogroove-array photocathodes that demonstrates understanding of both the engineering and the physical aspects of this advanced class of electron photoemitters. First, in Sec. II, we discuss the theory of plasmonic nanogroove photocathodes. In Sec. III, we explain the fabrication process and confirm the design dimensions by direct measurements of their optical properties. Nonlinear photoemission measurements performed on a 20-kV electron gun are reported in Sec. IV. We find the nonlinear photoemission coefficient for the nanostructured surfaces and are able to correlate its spread in values with the groove dimensions. We then confirm the polarization dependence of the photoemission and perform continuous measurement of average currents in excess of 100 nA to verify the enhanced electron yield and the photocathode stability. Lastly, in Sec. V, the mean transverse energy of the photocathode is characterized for different energies and the values found are compared with the behavior of the cathode at the surface. The paper then concludes by discussing future prospects for nanopatterned photoemitters.

## II. PRINCIPLES OF PLASMONIC NANOGROOVE PHOTOCATHODES

The ideal nanogroove cathode consists of a periodic array of trenches with depth  $d$  that extend infinitely in one direction and have nanometric width  $w$  in the other direction. We define a coordinate system used for the rest of this paper, with  $\hat{z}$  pointing normal to the cathode surface,  $\hat{y}$  running along the grooves, and  $\hat{x}$  against the grooves. Focusing for the moment on a single groove and imagining very large depth, light incident on the grooves may be coupled into modes within the gap that are best described by surface plasmon polaritons (SPPs) within a metal-insulator-metal waveguide [12] (the vacuum is the insulator in this case). These SPPs require additional momentum to couple with free-space illumination, owing to their dispersion relationship lying at larger wave vector for the same energy than the light line. For the case of the nanogrooves, the sharp edges at the entrance to the trenches can effectively provide such coupling [13]. The profile of the corner contains high-spatial-frequency components that allow light to diffract around it and onto the plasmon dispersion curve.

The finite depth of the groove acts to form a resonant Fabry-Perot-like cavity, with the allowable modes determined by the depth,  $d$ . The cavity depth that meets the resonance condition may be surprisingly small, only tens of nanometers for infrared light. This is explained by the fact that for the same energy, plasmons traveling along the walls of the gap may have an order of magnitude smaller wavelength than light in a vacuum [12]. The localization of optical energy to a nanometric region has the effect of field enhancement near the gap, which can exceed factors of 100 and favor nonlinear photoemission.

Figure 1(a) shows an example of local optical field enhancement by a nanogroove cathode computed using a finite-difference time-domain (FDTD) code. Specifically, LUMERICAL [14] is used in this work. Simulations are performed with periodic boundary conditions in the  $\hat{x}$  direction and excited by linearly polarized plane waves. The simulated cathode has grooves that are 14 nm wide, with a pitch of 680 nm, and is excited by light with a wavelength of 770 nm—representative of the cathodes studied in this paper. Figure 1(a) also shows the computed local variation of a static externally applied electric field.

The fact that emission occurs only at the sharp edges of the grooves may have an impact on the emittance of generated electron beams [10] and high local optical intensity can damage the gold surface [15]. However, the specific pattern used and the type and materials used during nanofabrication, such as the sharpness of the pattern, have an enormous impact on all of the above aspects.

The high quality factor (and narrow bandwidth) of the plasmonic nanogroove also have consequences for the photocathode response time. When the resonance bandwidth of the grooves is narrower than the bandwidth of the

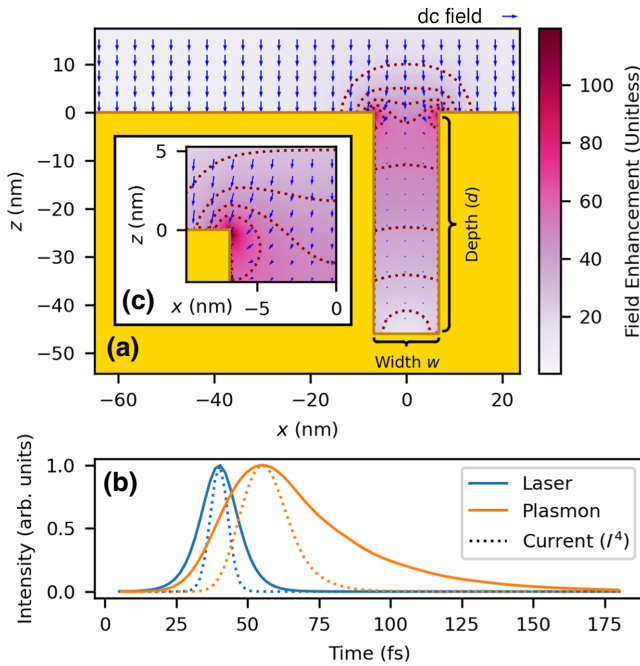


FIG. 1. (a) A plot (with contours) of the field enhancement around a cross section of the nanogroove structure. The solution is computed using an FDTD code [14]. The dc accelerating field, computed independently using a finite-difference code [16], is shown as the blue arrows. The inset [labeled (c)] shows a magnified view of the groove edge. (b) The time response of structure to a 15-fs excitation computed using FDTD (plasmon) compared to a flat surface (laser). The estimated current profiles are shown as dotted lines.

driving ultrafast laser, the field will continue to oscillate in the nanocavity longer than the duration of the excitation, effectively broadening the temporal response time of the cathode. An example of this effect is computed for the nanogroove-array photocathode in Fig. 1(a) by calculating the time-dependent field in response to excitation by ultrafast laser using the FDTD code in LUMERICAL [14]. The laser is 15 fs full width at half maximum (FWHM) and the calculated response of the structure is about 42 fs, or a factor of 3 longer [Fig. 1(b)]. The approximate bandwidth ( $\Delta\lambda$ ) and peak absorption wavelength ( $\lambda$ ) are 15 nm and 770 nm FWHM. The minimum time-bandwidth product of an approximately Gaussian pulse is 0.44 [17]. From this, an estimate of the optical time response can be calculated as

$$\Delta t_{\text{Response}} = \sqrt{\Delta t_{\text{Laser}}^2 + (a_1 a_2 \lambda^2 / (4\pi c \Delta\lambda))^2}, \quad (1)$$

where  $a_1$  and  $a_2$  are conversions from rms to FWHM values of the absorption bandwidth and nanogroove time response, respectively. Assuming Gaussian profiles, both  $a_1$  and  $a_2$  in Eq. (1) are approximately equal to 2.35, leading to a final cathode temporal response of approximately 50 fs FWHM. In order to obtain the extracted

electron-beam pulse duration, one would have to take into consideration the particular photoemission order used. In our case, the current density is proportional to the fourth order of the laser intensity, which suppresses the tails of the optical response and shrinks the final duration by a factor of 2 (for a Gaussian-like pulse). For ultrafast applications, other plasmonic cathode schemes that do not rely on resonant cavities may support higher bandwidths and allow use with even shorter laser pulses [18].

### III. CATHODE FABRICATION AND OPTICAL PROPERTIES

The photocathodes are fabricated out of gold using the template-stripping method [19,20]. While plasmonic structures can be fabricated using other methods, such as focused-ion-beam milling and the lift-off procedure, template stripping has been shown to yield superior surface roughness. Prior work has found rms roughness of 0.2 nm rms for template stripping compared to 1.4 nm for thermally evaporated metals [19]). A silicon wafer is UV and ozone cleaned for 5 min and spin coated with hydrogen silsesquioxane (HSQ) 2% resist. It is baked at 100°C for 1 min and then patterned using electron-beam lithography.

Cathodes with varying geometries are arranged in a square grids (a  $4 \times 4$  pattern) and multiple grids are imprinted along a single wafer, with an edge-to-edge distance of about 1 mm [see Figs. 2(b) and 2(c)]. The geometric dimensions of each of the 16 cathodes within a single square are varied, with a different groove pitch for each row and a different width for each of the four columns. The groove width is varied in part by controlling the electron dose, leaving some calibration required for this dimension. The groove depth is fixed by the fabrication procedure at

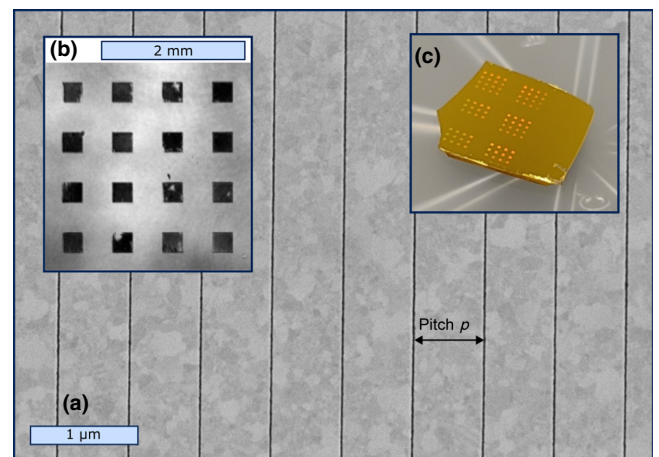


FIG. 2. (a) A scanning electron micrograph of the nanopatterned cathode. (b) A spatial image of the reflectance of 16 plasmonic nanogroove photocathodes contained in a single square of the sample. (c) An image of the fabricated cathode.

50 nm. After exposing the resist, the template is cleaned using RIE oxygen plasma for 30 s and 150 nm of gold is deposited. UV-curable epoxy is used to adhere a thin glass substrate to the gold and pressure causes this assembly (substrate, epoxy, and gold) to separate from the template, revealing the nanopatterned cathode.

The quality of the fabrication is first verified by imaging the surface via scanning electron microscopy [Fig. 2(a)] and confirming the close match between the array dimensions and the target values. The most centermost square grid is then used for optical and photoemission measurement as it is the easiest to align along the axis of the photoemission setup.

We then perform reflectivity measurements, starting with near-IR imaging, of all the 16 patterns across the selected square in the sample. We use a 770-nm-centered non-mode-locked Ti:sapphire laser oscillator as the illumination source. The linear laser polarization is tuned to point in the direction across the grooves (IE  $\hat{x}$ ), while the laser pulse hits the cathode at normal incidence. As can be qualitatively seen in Fig. 2(b), we observe strong suppression of the reflectivity in the regions that contain the nanopatterning.

The laser system is then mode locked and its full bandwidth is used to measure the reflectance spectra of the nanogroove photocathodes [see Fig. 3(d)]. Difference spectra are calculated using the beam reflected from the patterned surface against a reference pulse from an upstream 50:50 beam splitter for directions of linear polarization pointed along  $\hat{x}$  and  $\hat{y}$ . The reflected spectra for  $\hat{x}$  polarized light (i.e., against the grooves) are fitted to FDTD calculations [14] using the groove width for each of the 16 samples and a single overall angle of incidence as the free parameters. We find the best-fit angle of incidence for the cathode to be  $0.5^\circ$ . Figure 3(a) reports an example of a fit result for one cathode, exemplifying the close match found between the simulated and measured reflectance. The groove widths extracted are reported in Table I (fourth column) for all the cathodes in a square. From such results, we are able to confirm our fabrication methodology, as the width values increase with the column indices, i.e., with the electron-beam lithography dose, matching our expectations. The measured and simulated fit peak absorption wavelength and FWHM of the peak are compared in Figs. 3(b) and 3(c), showing excellent agreement.

Overall, these measurements demonstrate an ability to fabricate nanopatterned photocathodes with engineered optical properties.

#### IV. NONLINEAR PHOTOEMISSION FROM NANOPATTERNED CATHODE

In this section, we describe the measured nonlinear electron yield and average current of the nanogroove arrays.

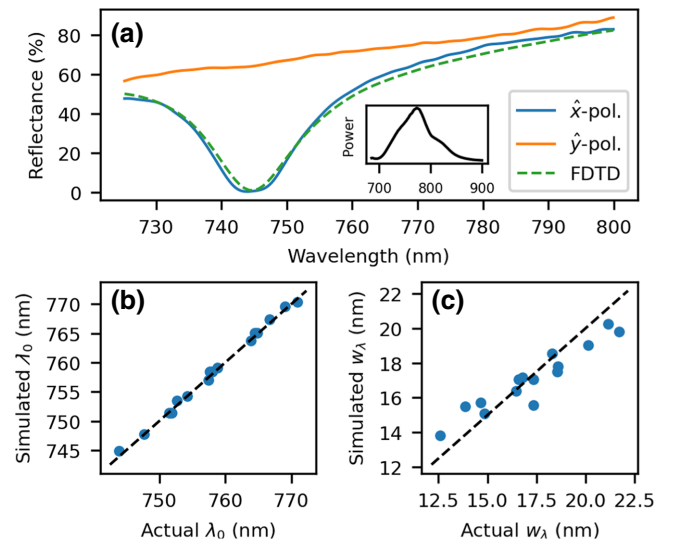


FIG. 3. (a) An example of reflectance spectra measured from one of the cathodes (670-nm pitch, 17.1-nm width) with a fit to the FDTD model using the groove width and the cathode tilt as the free parameters. (b) The peak absorption wavelength of the model and the measured grooves. (c) The FWHM of the absorption peak in the model and the fabricated sample. (d) The spectrum of the mode-locked driving laser.

The generalized Fowler-DuBridge model of multiphoton photoemission gives the scaling of  $n$ -photon current density,  $J_n$ , with laser intensity as the following

TABLE I. The dimensions of the nanogroove cathodes: the pitch ( $p$ ) and the groove width extracted from the fit of the reflectance spectra ( $w$ ). The measured effective nonlinear yield ( $a_4$ ) and the lower bound placed on the enhancement of the nonlinear yield over flat gold.

Row	Column	$p$ (nm)	$w$ (nm)	$a_4$ [(cm <sup>2</sup> A <sup>-1</sup> ) <sup>4</sup> ]	Enhancement bound
1	1	670	14.5	$3.0 \times 10^{-37}$	$7.5 \times 10^5$
1	2	670	14.5	$4.0 \times 10^{-38}$	$1.0 \times 10^5$
1	3	670	15.8	$2.3 \times 10^{-39}$	$5.7 \times 10^3$
1	4	670	17.1	$1.6 \times 10^{-38}$	$4 \times 10^4$
2	1	680	14.5	$8.9 \times 10^{-37}$	$2.2 \times 10^6$
2	2	680	14.5	$1.3 \times 10^{-37}$	$3.3 \times 10^5$
2	3	680	15.4	$1.0 \times 10^{-36}$	$2.5 \times 10^6$
2	4	680	16.2	$2.9 \times 10^{-37}$	$7.3 \times 10^5$
3	1	690	14.1	$3.0 \times 10^{-37}$	$7.5 \times 10^5$
3	2	690	14.1	$2.2 \times 10^{-37}$	$5.5 \times 10^5$
3	3	690	15.4	$2.2 \times 10^{-37}$	$5.5 \times 10^5$
3	4	690	15.8	$6.4 \times 10^{-39}$	$1.6 \times 10^4$
4	1	700	14.1	$4.5 \times 10^{-38}$	$1.1 \times 10^5$
4	2	700	13.7	$1.8 \times 10^{-37}$	$4.5 \times 10^5$
4	3	700	14.5	$5.8 \times 10^{-40}$	$1.5 \times 10^3$
4	4	700	15.4	$3.7 \times 10^{-39}$	$9.2 \times 10^3$

[7,21]:

$$J_n = a_n A_0 \left( \frac{e}{h\nu} (1 - R_\nu) I \right)^n T^2 F \left( \frac{nh\nu - e\phi}{k_B T} \right), \quad (2)$$

where  $a_n$  is a cathode-dependent constant representing the chance of multiphoton excitation,  $h$  is Planck's constant,  $k_B$  is the Boltzmann constant,  $e$  is the fundamental charge,  $\nu$  is the optical frequency,  $R_\nu$  is the reflectivity of the metal,  $\phi$  is the work function,  $I$  is the optical intensity,  $T$  is the temperature, and  $n$  is the order of emission. The value  $A_0 = 4\pi m_e k_B^2 e / h^3 \approx 120 \text{ A cm}^{-2} \text{ K}^{-2}$  is the Richardson constant, with  $m_e$  as the electron mass. The Fowler function can be written as  $F(x) = \int_0^\infty dy \ln(1 + \exp(-y - x))$ .

The literature value of  $\phi$  for gold is 5.4 eV [22]. Therefore, we expect fourth-order photoemission from the cathode when using 800-nm (1.54-eV) photons. Typical values for  $a_4$  of flat gold [23] lie around  $a_4 \approx 10^{-43} (\text{cm}^2 \text{ A}^{-1})^4$ . Previous work on nanopatterned gold has demonstrated nonlinear electron-yield enhancements of the order of  $10^6$  with picoampere-scale currents [20].

A schematic of our experimental setup for the measurement of electron beams from nanostructures is shown in Fig. 4. We transfer the nanopatterned wafers into a 20-kV electron gun and use the 80-MHz-repetition-rate mode-locked Ti:sapphire oscillator as the drive laser. The pulse is sent through a chirped-pulse compressor to achieve a Fourier-transform-limited pulse length of approximately 15 fs at the sample, also confirmed by autocorrelation measurements. The pulse is then focused to an rms spot size  $40 \mu\text{m}$  at the cathode plane with a small angle of incidence of  $4^\circ$  with respect to the surface normal. The intensity is varied using the combination of an achromatic half-wave plate and a polarizing beam splitter. The maximum laser energy that can be sent to the cathode after transport and longitudinal and transverse shaping is 1 nJ.

To begin, the polarizing beam splitter is temporarily removed and the half-wave plate is used to control the orientation of linear polarization of the laser. The photocurrent is measured from a single cathode using a lock-in amplifier and fitted to the model  $J(\theta) = A \cdot (\cos^2(\theta + \phi))^n + o$ , where  $A$  is the amplitude,  $o$  is an offset, and  $\phi$  is a phase to account for mispositioning of the half-wave plate in its rotation mount. The angle,  $\theta$ , is oriented so that  $0^\circ$  is close to  $\hat{x}$  in the coordinate system of the cathode. Our data and the line of best fit are shown in Fig. 5(c) and we conclude from the goodness of fit that only the polarization of light running “against the grain” of the grooves is able to excite plasmons and cause multiphoton photoemission, as expected.

The polarizing beam splitter is replaced and the emitted electron photocurrent is measured as a function of the optical intensity [Fig. 6(a)] for each of the cathodes in a square within the wafer. Equation (2) is then used in a fit to find

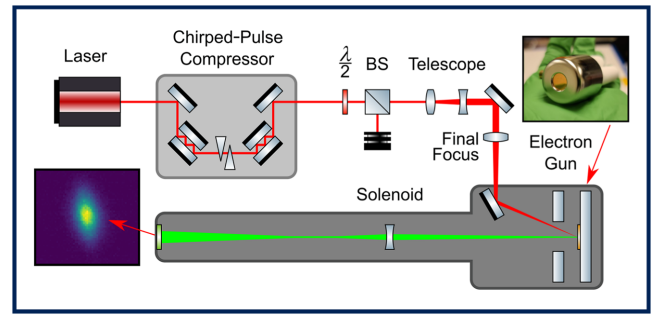


FIG. 4. A schematic of the beam line used in the measurements. An 80-MHz Ti:sapphire oscillator emits pulses centered around 770 nm. The light is sent through a chirped-pulse compressor for temporal compression and the beam is focused to a waist using a 600-mm-focal-length lens placed just before the window of the vacuum chamber. The intensity may be adjusted with a beam-splitter (BS) and half-wave-plate ( $\lambda/2$ ) pair. A telescope is used to expand the beam before hitting the lens to decrease its ultimate focused size. The electron beam emitted from the cathode is accelerated and sent through a solenoid lens before being imaged on a scintillator screen.

the nonlinear yield coefficient ( $a_4$ ), using 98% [22] as the value of the reflectivity of gold at 760 nm.

The distribution of the measured nonlinear yield exponents is shown in Fig. 6(e). All of the measured behavior is consistent with fourth-order photoemission. The measured value of the nonlinear yield coefficient varies from  $a_4 = 3 \times 10^{-40}$  to  $6 \times 10^{-37} (\text{cm}^2 \text{ A}^{-1})^4$ . A representation of its value distribution across the 16 cathodes in a square is shown in Fig. 6(b).

One explanation for the variation in  $a_4$  is the change in optical response of the grooves depending on their geometry [see Fig. 3(a)], which will change the overall coupling

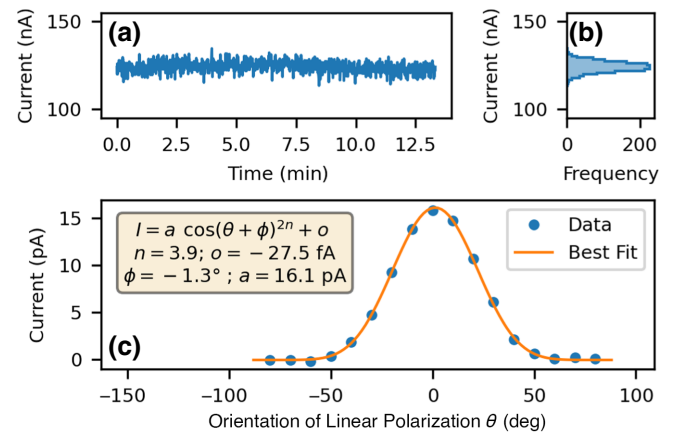


FIG. 5. (a) Time-series measurements of the photocurrent from a nanopatterned photocathode. (b) A histogram of the jitter in the photocurrent. (c) Measurements of the photocurrent as the angle of linear polarization is changed with the line of best fit.

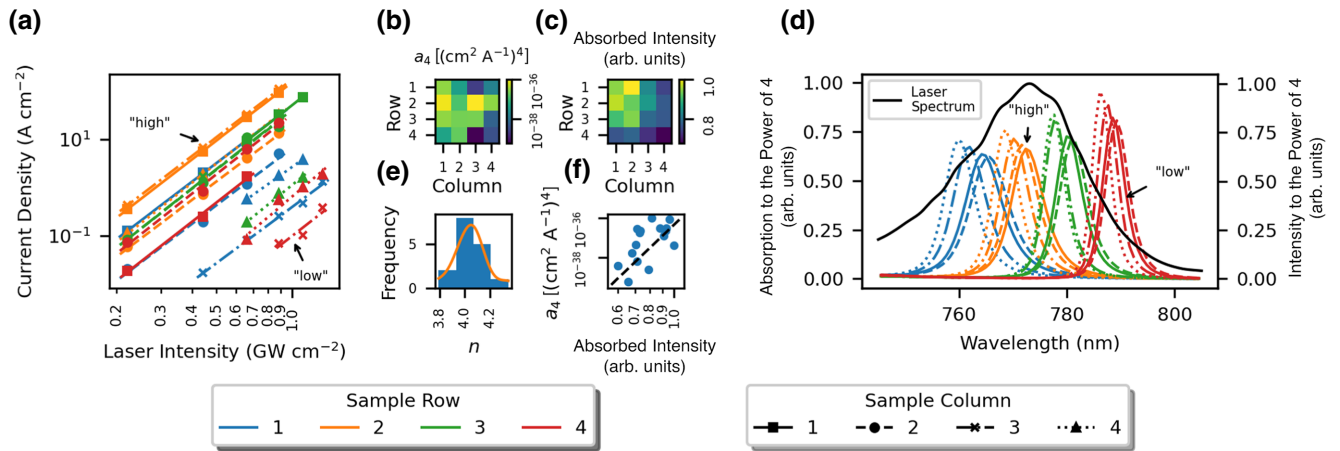


FIG. 6. (a) Measurements of the photocurrent as the laser intensity is varied, with power-law fits shown as lines. (b) The best-fit yield  $[a_n$  in Eq. (2)], laid out by location on the  $4 \times 4$  grid of cathodes [Fig. 2(b)]. (c) An estimate of the absorbed laser intensity, laid out by its location in the grid and log scaled. (d) the fourth power of the nanogroove absorption overlaid with the spectrum of the laser. (e) The distribution of the best-fit exponents in the power-law curves (blue, histogram; orange, kernel density estimator). (f) A scatter plot of the yield ( $a_4$ ) and the estimated absorbed laser intensity. The colors and line style used in (a) and (d) indicate the sample location and high- and low-yield examples are highlighted.).

of the laser power into the structure. Depending on the value of the peak absorption wavelength, the reflectance curve will align better or worse with the power spectrum of the laser [Fig. 6(d)], changing the amount of total absorbed intensity from the laser that then excites electrons in the metal. The yield should be related to the fourth power of the absorbed intensity, which can be estimated as the integral

$$(\text{Abs. Int.})^4 = \left[ \int_0^\infty I(\lambda) \cdot A(\lambda) d\lambda \right]^4,$$

where  $I(\lambda)$  is the spectrum of the laser and  $A(\lambda)$  is the absorption spectrum of the nanogroove. Indeed, if we evaluate this integral numerically [Fig. 6(c)] for each groove array, we observe a correlation [Fig. 6(f)].

The current emission from the flat (nonpatterned) gold surface is below our measurement sensitivity, owing to the limited available optical intensity in the setup. Nevertheless, with a maximum power density achievable of approximately  $2 \text{ GWcm}^{-2}$ , and a measurement system noise floor of approximately  $50 \text{ fA}$ , we can calculate an upper bound for the nonlinear yield coefficient of  $a_4 < 4 \times 10^{-43} (\text{cm}^2 \text{A}^{-1})^4$ , with a yield enhancement from nanopatterning in excess of  $10^6$ . This bound agrees with previous measurements on identically prepared flat gold that have found  $a_4 = 1 \times 10^{-43} (\text{cm}^2 \text{A}^{-1})^4$  [24].

The current stability of the cathode performance is summarized in Fig. 5. A continuous acquisition of average electron current values over about 12 min is performed, with the laser pulses delivering the maximum available energy [Fig. 5(a)]. A stable average-current value of 120

nA is measured, with fluctuations measured to be 2.3% [see Fig. 5(b)].

This experiment exemplifies the disruptive potential of the technology in high-average-current electron sources. Indeed, assuming a gold UV quantum efficiency of  $10^{-5}$  [25] and a typical conversion efficiency from near-infrared (NIR) to UV of 7.5%, then linear photoemission would require a tenfold increase in laser power to generate the same average current, about 0.75 W in the NIR against the 80 mW used in the experiment.

## V. MEAN TRANSVERSE ENERGY OF THE EMITTED ELECTRON BEAM

In this section, we explore the mean transverse energy (MTE) [26] of the nanogroove cathodes. After showing that surface nanopatterning can lead to very large nonlinear yield enhancements in metals, we now seek to explore the effects of such enhancement on the transverse brightness of the beam. Early work on nanopatterned photocathodes has found larger emittance values than are expected from a flat surface [10]. Since then, substantial work tailored at improving the photoemission properties of these cathodes has been carried out, e.g., by selecting and optimizing the fabrication technique for minimal roughness and sharp patterns and by developing methods for *in situ* optical characterization of the structures [18]. Owing to such developments, we are now able to relate photoemission properties such as the cathode electron-beam MTE to the surface mechanical and optical characteristics.

We investigate the transverse emittance of the grooves using the solenoid-scan method. The electron gun is biased at high voltage to generate a beam from one of the cathodes

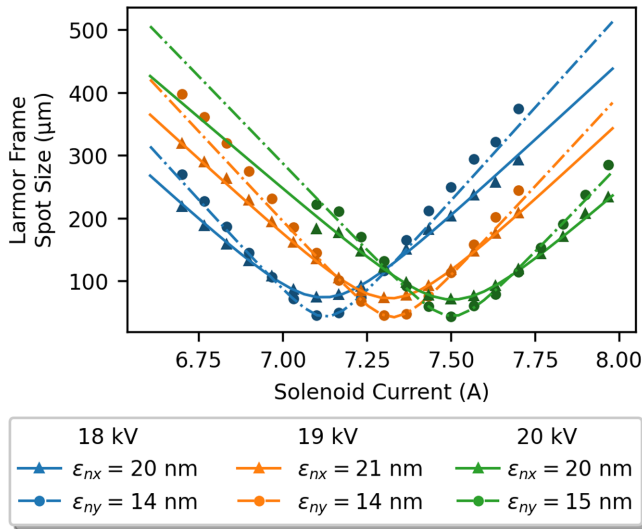


FIG. 7. Solenoid-scan measurements of the normalized emittance of the generated beam. The size of the beam (shown here in the Larmor frame) is measured as a function of the current in the beam-line solenoid. Fits to a linear model of the beam line are shown as the curves, with the best-fit emittance in the legend.

in the square [row two and column one in Fig. 2(b); 680-nm pitch and 14.5-nm width]. The generated electron beam passes through a solenoid lens a few centimeters away from the cathode and hits a scintillator screen 60 cm away. Here, the rms spot size of the beam is measured as a function of the strength of the solenoid lens. The experiment is repeated at 20, 19, and 18 kV (data shown in Fig. 7) and the beam sizes are fitted using a linear model of transport including the accelerating electric field in the gun, following the procedure in Refs. [6,27], to recover the initial phase-space moments. The laser rms spot size at the cathode is measured to be 20  $\mu\text{m}$ . We find the cathode MTE to be asymmetric, with  $\text{MTE}_x = 510$  meV and  $\text{MTE}_y = 250$  meV. The  $x$  and  $y$  axes are as before, with  $\hat{x}$  running against the grooves and  $\hat{y}$  running along them. The MTE along  $\hat{y}$  is close to what is typical for a flat metal with this excess energy [28]. On the other hand, the MTE in the horizontal ( $x$ ) plane shows a substantial increase, which we attribute to geometric effects, as described below.

While nanopatterning has clear benefits for the nonlinear yield of photocathodes, those same nanoscale features are a form of surface roughness, which is well known to cause an increase in the MTE of the emitted electrons from a photocathode [29]. Two major effects contribute to this increase: the additional transverse momentum gained from the local distortions of electric fields around surface features (as in Fig. 1) and the local deviation of the average direction of photoemission with respect to the global beam-line axis, which follows the surface normal. For nanogroove photocathodes, these effects will vanish in one direction ( $\hat{y}$  in our setup), due to the translational symmetry

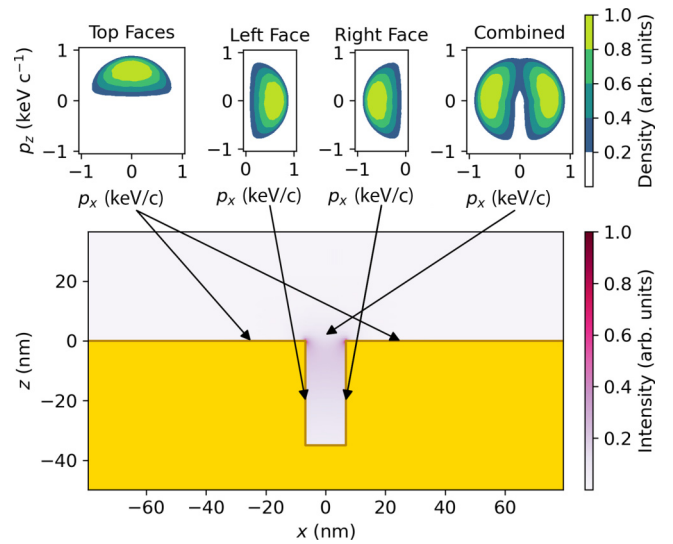


FIG. 8. A schematic showing how the initial momentum distribution (measured in units of  $\text{keV}/c$ , where  $c$  is the speed of light) from each face of the nanogroove may be combined to form an estimate of the MTE including roughness effects.

of the structure. To understand the increase of emittance on the horizontal ( $x$ ) axis, we now estimate the contribution of both effects in our setup.

For the first effect, we compute the value of the externally applied electric field around the nanogrooves using the finite-difference method [16], assuming perfect edges (i.e., a radius of curvature equal to the simulation mesh size). This is shown as the blue arrows in Fig. 1(a). We then compute the integral of the transverse field along the particle trajectory, starting from the groove edge, to find the maximum transverse energy acquired by the electrons. For the maximum achievable cathode field in the gun (which will maximize this effect) of  $7 \text{ MV m}^{-1}$ , this effect only adds approximately 10 meV of transverse energy to the emitted electrons.

To estimate the effect of the local variations of the surface normal on the MTE, we start by randomly sampling the three-dimensional momentum distribution of electrons emitted from a flat metallic surface [28], generating a set of 100 000 virtual particles. Assuming a work function for gold of 5.4 eV [30] and a fourth-order photoemission process, a numerical calculation of the MTE of these particles gives a value of 257 meV, in close accordance with our measurement in the vertical plane and the analytical expression  $\text{MTE} = (nh\nu - \phi)/3$ . Rotating the distribution following the local normal to the surface and adding together all of the contributions, we can obtain an estimate of the total MTE including the effect of nanopatterning. The number of electrons emitted from each nanogroove face along the surface is weighted by the integral of the fourth power of the intensity along it, extracted by FDTD simulations [Fig. 1(a)]. This gives a ratio of side wall to top

emission of 6.9:1 and a total estimated MTE, with normal vector effects included, of 481 meV. Adding in the approximately 10 meV calculated above due to the effects of the transverse fields, this approaches our measured value in the horizontal plane of 510 meV. A visual of how this estimate is made can be found in Fig. 8.

## VI. CONCLUSIONS

In this work, we report the development and engineering of a nanopatterned metal photocathode for high-brightness ultrafast electron generation. We demonstrate increased average current when using plasmon-assisted multiphoton photoemission with respect to linear photoemission in our setup, overcoming the major drawbacks of metal cathodes caused by their poor quantum efficiency (QE) in the UV and hopefully paving the way for their use in high-average-current–high-brightness applications, such as x-ray free-electron lasers (x-FEL) and ultrafast electron diffraction (UED) setups.

Our fabricated cathodes closely match their designed optical performance. In particular, we are able to tune the peak absorption wavelength of the structure to the spectral peak of the driving laser.

The electron yield is strongly enhanced via surface nanostructuring, a factor in excess of  $10^6$  over fourth-order photoemission from flat gold, and a reduction in power by a factor of approximately 10 compared to linear photoemission for the intensities achieved in this work. Continuous operations at high average current show no degradation [Fig. 5(a)]. To showcase the potential impact of such nanopatterned cathodes, we compare their requirements with typical metal photocathodes used in large-scale facilities. As an example, The Linac Coherent Light Source (LCLS) x-FEL at the SLAC National Accelerator Laboratory [31] uses linear photoemission from flat copper cathodes. By using the operational values for the laser, cathode QE, and beam charge [32,33] (3 ps FWHM, 150-pC pulse from a 1-mm hard-edge spot size, a QE of  $4 \times 10^{-5}$ ), and a typical operational conversion efficiency from IR to UV of 7.5%, a flat copper cathode requires about 240  $\mu\text{J}$  of energy in the IR pulse, compared to the 8  $\mu\text{J}$  necessary for the gold nanostructured photocathode presented here. The advantage of nanopatterning becomes even more pronounced in applications requiring low charge and femtosecond-long pulses, such as UED setups [34]. In the example shown in Fig. 5(a), 1.5-fC electron beams are produced using only 1 nJ of IR energy, extracted directly from an ultrafast laser oscillator.

The normalized transverse emittance of the photoemitted beam is measured systematically for different beam energies, providing a benchmark value for the transverse brightness of nanopatterned cathodes. The measured asymmetry in the emittance can be fully explained by the geometry of the structure, with its asymmetric roughness. These

results suggests an interesting application of nanogroove arrays as a future platform for studying the effects of roughness on electron source brightness. In these systems, the roughness can be engineered to take on certain profiles. Further, the fact that the cathode “acts flat” in one direction provides a control measurement to directly compare the effects of roughness against in each sample. For the application of cathodes in high-brightness photoinjectors, although the emittance is increased in the direction normal to the grooves, it is still in line or better than typical values measured in ultrafast x-ray user facilities [4].

An interesting future application of emission from patterned surfaces is the possibility of obtaining transverse electron-beam density modulation and shaping. Since electrons are only emitted near the groove edges, structures could be engineered to generate nanoscale beamlets and density modulations. Using linear optics to perform an emittance exchange [35], this modulation can be transferred into time and used to drive temporal patterning of the beam, which is of interest to coherent x-ray light sources [36]. Also, a round beam [37,38] could be generated to average out the emittances in both directions.

To further reduce the emittance from plasmonic photocathodes, emission from a flat surface would be required, e.g., by using a plasmonic lens, as described in Ref. [18], where surface-plasmon interference is used to produce large and instantaneous field enhancements in pattern-free areas well below 1  $\mu\text{m}$ . The implementation of this design could improve the transverse brightness from metal cathodes even further over the state of the art.

## ACKNOWLEDGMENTS

C.M.P. acknowledges U.S. National Science Foundation (NSF) Award No. PHY-1549132, the Center for Bright Beams, and the U.S. Department of Energy (DOE) Office of Science Graduate Student Research (SCGSR) program. D.F. acknowledges support from the Office of Science, Office of Basic Energy Sciences, of the U.S. DOE, under Contract No. DE-AC02-05CH11231. Work at the Molecular Foundry was supported by the Office of Science, Office of Basic Energy Sciences, of the U.S. DOE, under Contract No. DE-AC02-05CH11231. D.B.D. and A.M.M. acknowledge support from the NSF Science and Technology Center on Real-Time Functional Imaging (STROBE) under Grant No. DMR-1548924, which included funds for building the laser transport line in the dc photoemission test stand used in this work.

## APPENDIX: SENSITIVITY OF REFLECTANCE TO LASER ANGLE OF INCIDENCE

In Sec. III, the laser angle of incidence is used as one of the free parameters when fitting the FDTD simulations to measurements of reflectivity (i.e., Fig. 3). Given the requirement that the angle of incidence should be the same



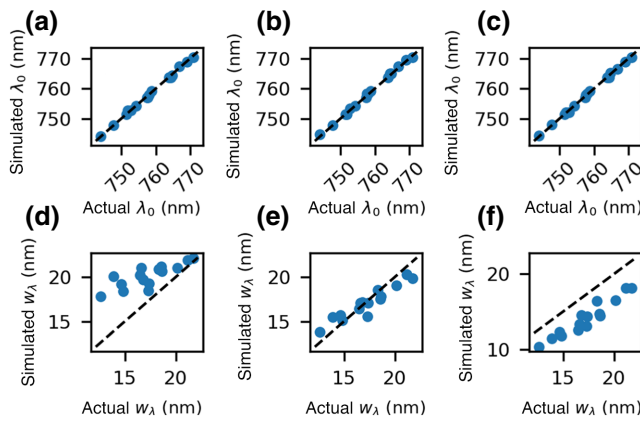


FIG. 9. The variation of the modeled nanogroove reflectivity as the laser angle of incidence is varied: (a),(d)  $\theta = 0.0$ ; (b),(e)  $\theta = 0.5$ ; (c),(f)  $\theta = 1.0$ . The parameters of the reflectivity peaks compared with the measurements [as in Figs. 3(b) and 3(c)] are shown for a few angles compared with the best-fit value of  $\theta$ , given in (b) and (e).

across all 16 nanogroove samples on the wafer, a best-fit value of  $\theta = 0.5$  is found and the best-fit simulations agree closely with our measurements. To better understand the effect of this angle on our results, we repeat the analysis, but for several fixed angles of incidence. These results are summarized in Fig. 9.

The main impact of changing the angle of incidence is to change the width of the absorption peaks without affecting their location. This suggests that the groove width, which does change the location of the peak and is the only remaining free parameter, can be accurately predicted from data even when there is uncertainty in the tilt of the cathode. Confirming this, the best-fit groove width varies on average by only 5% as the angle is varied in Fig. 9.

Additionally, we propose in Sec. IV that aligning the absorption peak with the spectrum of the driving laser is important to optimize the performance of the cathode. Since the position of the absorption peak of the cathode does not change much with the angle of incidence, the nonlinear yield should be equally robust. This is a useful property for applications where engineering constraints place limits on how well the angle of incidence of the laser can be known.

- [1] LCLS-II Project Team, *LCLS-II Final Design Report*, Tech. Rep. LCLSII-1.1-DR-0251-R0 (SLAC, 2015).
- [2] M. Altarelli, K. Brinkmann, M. Chergui, W. Decking, and B. Dobson, *XFEL, the European X-Ray Free-Electron Laser: Technical Design Report*, Tech. Rep. DESY 2006-097 (DESY XFEL Project Group, Hamburg, 2006).
- [3] E. Prat and S. Bettoni, in *Proceedings of FEL2014* (JACoW Publishing Group, Basel, Switzerland, 2014), p. 6.

- [4] R. Akre, D. Dowell, P. Emma, J. Frisch, S. Gilevich, G. Hays, P. Hering, R. Iverson, C. Limborg-Deprey, H. Loos, A. Miahnahri, J. Schmerge, J. Turner, J. Welch, W. White, and J. Wu, Commissioning the Linac Coherent Light Source injector, *Phys. Rev. Spec. Top.—Accel. Beams* **11**, 030703 (2008).
- [5] J. K. Bae, I. Bazarov, P. Musumeci, S. Karkare, H. Padmore, and J. Maxson, Brightness of femtosecond nonequilibrium photoemission in metallic photocathodes at wavelengths near the photoemission threshold, *J. Appl. Phys.* **124**, 244903 (2018).
- [6] I. V. Bazarov, B. M. Dunham, Y. Li, X. Liu, D. G. Ouzounov, C. K. Sinclair, F. Hannon, and T. Miyajima, Thermal emittance and response time measurements of negative electron affinity photocathodes, *J. Appl. Phys.* **103**, 054901 (2008).
- [7] P. Musumeci, L. Cultrera, M. Ferrario, D. Filippetto, G. Gatti, M. S. Gutierrez, J. T. Moody, N. Moore, J. B. Rosenzweig, C. M. Scoby, G. Travish, and C. Vicario, Multiphoton Photoemission from a Copper Cathode Illuminated by Ultrashort Laser Pulses in an rf Photoinjector, *Phys. Rev. Lett.* **104**, 084801 (2010).
- [8] J. Krüger, D. Dufft, R. Koter, and A. Hertwig, Femtosecond laser-induced damage of gold films, *Appl. Surf. Sci.* **253**, 7815 (2007).
- [9] A. Polyakov, C. Senft, K. F. Thompson, J. Feng, S. Cabrini, P. J. Schuck, H. A. Padmore, S. J. Peppernick, and W. P. Hess, Plasmon-Enhanced Photocathode for High Brightness and High Repetition Rate X-Ray Sources, *Phys. Rev. Lett.* **110**, 076802 (2013).
- [10] R. K. Li, H. To, G. Andonian, J. Feng, A. Polyakov, C. M. Scoby, K. Thompson, W. Wan, H. A. Padmore, and P. Musumeci, Surface-Plasmon Resonance-Enhanced Multiphoton Emission of High-Brightness Electron Beams from a Nanostructured Copper Cathode, *Phys. Rev. Lett.* **110**, 074801 (2013).
- [11] Y. Gong, A. G. Joly, L. Kong, P. Z. El-Khoury, and W. P. Hess, High-Brightness Plasmon-Enhanced Nanostructured Gold Photoemitter, *Phys. Rev. Appl.* **2**, 064012 (2014).
- [12] J. Le Perchec, P. Quémerais, A. Barbara, and T. López-Ríos, Why Metallic Surfaces with Grooves a Few Nanometers Deep and Wide May Strongly Absorb Visible Light, *Phys. Rev. Lett.* **100**, 066408 (2008).
- [13] A. Polyakov, S. Cabrini, S. Dhuey, B. Harteneck, P. J. Schuck, and H. A. Padmore, Plasmonic light trapping in nanostructured metal surfaces, *Appl. Phys. Lett.* **98**, 203104 (2011).
- [14] LUMERICAL, finite difference time domain solutions (2011).
- [15] A. Polyakov, Ph.D. thesis, UC Berkeley, Berkeley, California, 2012.
- [16] M. Menzeland H. Stokes, *User's Guide for the POISSON/SUPERFISH Group of Codes*, Tech. Rep. LA-UR-87-115 (Los Alamos National Laboratory, Los Alamos, New Mexico, 1987).
- [17] J.-C. Diels and W. Rudolph, *Ultrashort Laser Pulse Phenomena: Fundamentals, Techniques, and Applications on a Femtosecond Time Scale*, Optics and Photonics (Academic Press, Burlington, Massachusetts, 2006), 2nd ed.
- [18] D. B. Durham, F. Riminucci, F. Ciabattini, A. Mostacci, A. M. Minor, S. Cabrini, and D. Filippetto, Plasmonic Lenses

- for Tunable Ultrafast Electron Emitters at the Nanoscale, *Phys. Rev. Appl.* **12**, 054057 (2019).
- [19] N. Vogel, J. Zieleniecki, and I. Köper, As flat as it gets: Ultrasoother surfaces from template-stripping procedures, *Nanoscale* **4**, 3820 (2012).
- [20] A. Polyakov, H. A. Padmore, X. Liang, S. Dhuey, B. Harteneck, J. P. Schuck, and S. Cabrini, Light trapping in plasmonic nanocavities on metal surfaces, *J. Vac. Sci. Technol. B, Nanotechnol. Microelectron.: Mater., Process., Meas., Phenom.* **29**, 06FF01 (2011).
- [21] G. Ferrini, F. Banfi, C. Giannetti, and F. Parmigiani, Non-linear electron photoemission from metals with ultrashort pulses, *Nucl. Instrum. Methods Phys. Res. Sect. A: Accelerators, Spectrometers, Detectors Associated Equipment* **601**, 123 (2009).
- [22] M. Bass, *Handbook of Optics* (McGraw-Hill Professional, New York, 2000).
- [23] V. Schweikhard, A. Grubisic, T. A. Baker, and D. J. Nesbitt, Multiphoton scanning photoionization imaging microscopy for single-particle studies of plasmonic metal nanostructures, *J. Phys. Chem. C* **115**, 83 (2011).
- [24] D. B. Durham, S. Rotta Loria, F. Riminucci, K. Kanellopoulos, X. Shen, F. Ciabattini, A. Mostacci, P. Musumeci, A. M. Minor, S. Cabrini, and D. Filippetto, in *Plasmonics: Design, Materials, Fabrication, Characterization, and Applications XVIII*, edited by T. Tanaka and D. P. Tsai (SPIE, Online Only, Bellingham, Washington, 2020), p. 71.
- [25] J. Fischer and T. Srinivasan-Rao, in *Proceedings of the Workshop on Pulse Power Techniques for Future Accelerators* (Erice, Italy, 1988), p. 26.
- [26] H. Lee, S. Karkare, L. Cultrera, A. Kim, and I. V. Bazarov, Review and demonstration of ultra-low-emittance photocathode measurements, *Rev. Sci. Instrum.* **86**, 073309 (2015).
- [27] C. Gulliford and I. Bazarov, New method for generating linear transfer matrices through combined rf and solenoid fields, *Phys. Rev. Spec. Top.—Accel. Beams* **15**, 024002 (2012).
- [28] D. H. Dowell and J. F. Schmerge, Quantum efficiency and thermal emittance of metal photocathodes, *Phys. Rev. Spec. Top.—Accel. Beams* **12**, 074201 (2009).
- [29] D. J. Bradley, M. B. Allenson, and B. R. Holeman, The transverse energy of electrons emitted from GaAs photocathodes, *J. Phys. D: Appl. Phys.* **10**, 111 (1977).
- [30] H. B. Michaelson, The work function of the elements and its periodicity, *J. Appl. Phys.* **48**, 6 (1977).
- [31] P. Emma *et al.*, First lasing and operation of an ångstrom-wavelength free-electron laser, *Nat. Photonics* **4**, 641 (2010).
- [32] F. Zhou, A. Brachmann, P. Emma, S. Gilevich, and Z. Huang, Impact of the spatial laser distribution on photocathode gun operation, *Phys. Rev. Spec. Top.—Accel. Beams* **15**, 090701 (2012).
- [33] F. Zhou, J. Sheppard, T. Vecchione, E. Jongewaard, A. Brachmann, J. Corbett, S. Gilevich, and S. Weathersby, Establishing reliable good initial quantum efficiency and in-situ laser cleaning for the copper cathodes in the RF gun, *Nucl. Instrum. Methods Phys. Res. Sect. A: Accelerators, Spectrometers, Detectors Associated Equipment* **783**, 51 (2015).
- [34] D. Filippetto, P. Musumeci, R. K. Li, B. J. Siwick, M. R. Otto, M. Centurion, and J. P. F. Nunes, Ultrafast electron diffraction: Visualizing dynamic states of matter, *Rev. Mod. Phys.* **94**, 045004 (2022).
- [35] E. Nanni, W. Graves, and D. Moncton, Nanomodulated electron beams via electron diffraction and emittance exchange for coherent x-ray generation, *Phys. Rev. Accel. Beams* **21**, 014401 (2018).
- [36] W. S. Graves, F. X. Kärtner, D. E. Moncton, and P. Piot, Intense Superradiant X Rays from a Compact Source Using a Nanocathode Array and Emittance Exchange, *Phys. Rev. Lett.* **108**, 263904 (2012).
- [37] Y. Derbenev, *Untitled Report*, Tech. Rep. UMHE-98-04 (University of Michigan, 1998).
- [38] R. Brinkmann, Y. Derbenev, and K. Flöttmann, A low emittance, flat-beam electron source for linear colliders, *Phys. Rev. Spec. Top.—Accel. Beams* **4**, 053501 (2001).